AIMS Materials Science, 11(6): 1083–1095.
DOI: 10.3934/matersci.2024052
Received: 18 June 2024
Revised: 05 November 2024
Accepted: 11 November 2024
Published: 25 November 2024

https://www.aimspress.com/journal/Materials

Research article

Research on the oxidation sequence of Ni-Al-Pt alloy by combining experiments and thermodynamic calculations

Na Ta[1,*], Lijun Zhang[2] and Qin Li[2]

[1] School of Materials Science and Engineering, University of Science and Technology Beijing, Beijing 100083, China
[2] State Key Laboratory of Powder Metallurgy, Central South University, Changsha 410083, China

* **Correspondence:** Email: tagetacpu@163.com; tana@ustb.edu.cn; Tel: +86-185-1921-4296.

Abstract: In this paper, a comprehensive study on 1373 K high-temperature oxidation behaviors in a Ni-20 at.% Al-5 at.% Pt system was performed by coupling experimental investigations with CALPHAD (CALculation of PHAse Diagram) calculations. The discussion was expanded to include the effects of chemical concentrations on the degradation mechanism of thermally grown oxide layers during oxidation at 1373 K. A step-by-step oxidation procedure was established: first, aluminum oxide grows on the underside, followed by nickel oxide, which fully develops and penetrates the original aluminum oxide. The formation of NiO leads to aluminum enrichment and nickel depletion; once the concentration of Al achieves a threshold, θ-Al_2O_3 transforms into α-Al_2O_3, forming a tight structure. At this point, Al diffusion toward the exterior predominates, followed by the inward diffusion of O. The diffusion of Ni is gradually restricted by the establishment of the α-Al_2O_3 layer. When Al is not enough, Al_2O_3 combines with NiO to develop $NiAl_2O_4$. Nickel segregation may also occur during subsequent oxidation at the oxide layer/matrix alloy boundary. Small voids are likely to form due to the merging of the vacancies caused by the unbalanced diffusion of Al toward the Al_2O_3 layer and the opposite diffusion of Ni, resulting in significant peeling failure. Additionally, Pt has a beneficial effect by forming a thinner oxide scale that is more resistant to spallation.

Keywords: Ni-Al-Pt; high-temperature oxidation; CALPHAD; NiO; Al_2O_3

1. Introduction

As an important intermediate transitional scale between the ceramic coat and substrate alloy in thermal barrier coatings (TBCs), the bond coat is easily oxidized and forms a thermally grown oxide (TGO) scale [1], whose continuity and stability determines the failure life of TBC materials. Once the aluminum is severely depleted due to simultaneous consumption by both oxidation and inward diffusion into the matrix alloy, the TGO layer undergoes extensive scale spallation [2]. While the Al concentration decreases beneath a threshold value, a complete and steady Al_2O_3 scale may develop, finally resulting in the failure and rupture of the oxide layer. Hence, a continuously porous-free, good TGO layer with excellent adhesion should be established during the oxidation of the bond coat.

The latest γ/γ′ Ni-based alloys with Pt addition have become promising bond coats [3,4], benefiting from their up-diffusion phenomenon; the presence of Pt can facilitate the transfer of Al from the matrix alloy to the bond coat, ensuring adequate Al levels [5–8]. Several studies [9–12] have investigated the influence of Pt on oxidation behavior. It has been found that Pt suppresses the diffusion of elements from the matrix to the surface, thus contributing to the stable development of α-Al_2O_3 and effectively avoiding the detrimental oxide formation around the TGO interface [13–15]. Additionally, Pt reduces chemical activity, thus effectively slowing down the failure process [16]. It has been demonstrated that Pt modification results in oxygen diffusion into the metallic substrate, as demonstrated through internal oxidation experiments on the Ni-20 at.% Al-3 at.% Pt alloy at 1423 K [17]. When the addition of Pt is increased high enough, usually higher than 15 at.%, the chemical activity of Al declines, leading to the uphill diffusion of Al in the matrix alloy.

Considering the deleterious effects of brittle nickel oxides (NiO and $NiAl_2O_4$) on the TGO layer, they have been widely studied [18]. Xiao et al. [19] investigated the high-temperature oxidation process in several γ/γ' alloys with different Pt contents (0, 10, and 15 at.%). As previously mentioned, Pt has a strong preference for specific sites within the Ni crystal lattice in the L_{12} configuration and tends to migrate to the alloy surface due to its larger atomic radius compared to Ni. This increases the effective Al/Ni atomic ratio in specific crystallographic planes [20], promoting the formation of α-Al_2O_3 instead of NiO. Consequently, a preferential TGO layer formation is influenced not only by alloy composition and phase structure but also by the diffusion of other elements toward the oxidation interface during service.

Based on previous research, the latest generation of Ni-Al-Pt alloy bond coats was chosen as the research focus to obtain a more detailed understanding of bond coat oxidation behavior and its up-diffusion protection effect. In this study, an experimental program combined with thermodynamic calculations of chemical activity was conducted to acquire a deeper understanding. The effects of alloy composition on TGO layer degradation behavior during oxidation experiments at 1373 K were investigated and discussed.

2. Materials and methods

Arc melting was used to prepare Ni-20 at.% Al-5 at.% Pt target alloys with unstained Ni, Al, and Pt metals (99.999%) in a vacuum atmosphere. After arc melting, the alloy was treated in inert gas and then annealed for 336 h at 1373 K in a vacuum. Specimens were fabricated into discs with 2 mm thickness and polished with SiC paper up to 2000 mesh. A thin oxidation film was removed by cleaning with a mixture of acid (99%) and H_2O in a 1:6 ratio for 5 min. Oxidation experiments were conducted

on a GSL-1700X high-temperature vacuum tube furnace. The experimental temperature was set to 1373 K, the exposure time to 130 h, and the oxygen partial pressure was PO_2 = 0.21 bar. Prior to exposure, the temperature of the furnace was increased to 1373 K at a rate of 20 ℃/min. After 130 h of oxidation, specimens were mechanically polished using a 1 μm abrasive paste. Then, specimens were desiccated and stored in glassware for subsequent characterization using an electron-probe microanalyzer (EPMA), scanning electron microscope (SEM) for microstructural analysis, and X-ray diffraction (XRD). Energy-dispersive X-ray spectroscopy was used to measure and confirm the alloy composition.

3. Results and discussion

3.1. Experimental characterization of oxidation

Figure 1 shows the detailed microstructure and phase distribution in the TGO scales of the Ni-20 at.% Al-5 at.% Pt alloy after oxidation for 130 h at PO_2 partial pressure of 0.21 bar at 1373 K. SEM images with different contrasts illustrate the thickness of the oxide layer, which is approximately 7–8 μm. In Figure 1a, a homogenous γ-Ni secondary surface area with darker contrast is observed around the oxide scales due to the quick diffusion of aluminum, forming an Al_2O_3 layer approximately 45.90 μm thick.

The formation of Al_2O_3 in the TGO scale led to the depletion of aluminum in the substrate alloy. On the other hand, the consumption of aluminum during the oxidation process affected the mechanical properties of the substrate alloy, influencing the lifespan of the entire coating system. For instance, the formation of $NiAl_2O_4$ phases under adverse conditions contributed to interfacial brittleness. Figure 1a,c show a 5–12 μm thick zone of internal oxidation near the interface with the Ni-Al-Pt matrix alloy, where internal oxide particles are visible in the substrate alloy. The presence of different oxide phases in the TGO layers is indicated by contrast in the SEM/BSE (Backscattered Electron) images, suggesting a need for additional compositional analysis. The particular morphology of the γ'/γ phases in the oxidized alloys is shown in Figure 2, indicated by the bright contrasts. As shown in Figure 2b, the dark channel region displays a reticular structure with γ and γ' blocks embedded in each other.

The composition of the oxidation layer was detected by energy dispersive spectroscopy (EDS), with measurements taken along two lines across the oxide layer marked in red in Figure 1c,d. While the precision of EDS measurement is not enough to characterize light atoms, the results provide qualitative insights. The EDS analysis curve in Figure 3 shows a nickel content of approximately 50–60 at.% in the oxide layer, while in the central region, the detected ratio of O to Ni approaches 1:1, suggesting the presence of NiO. In addition, traces of metallic Ni or Ni_3Al may be present, based on the EDS map. Therefore, the oxide layer consists of a mixture of different phases and oxidation compounds.

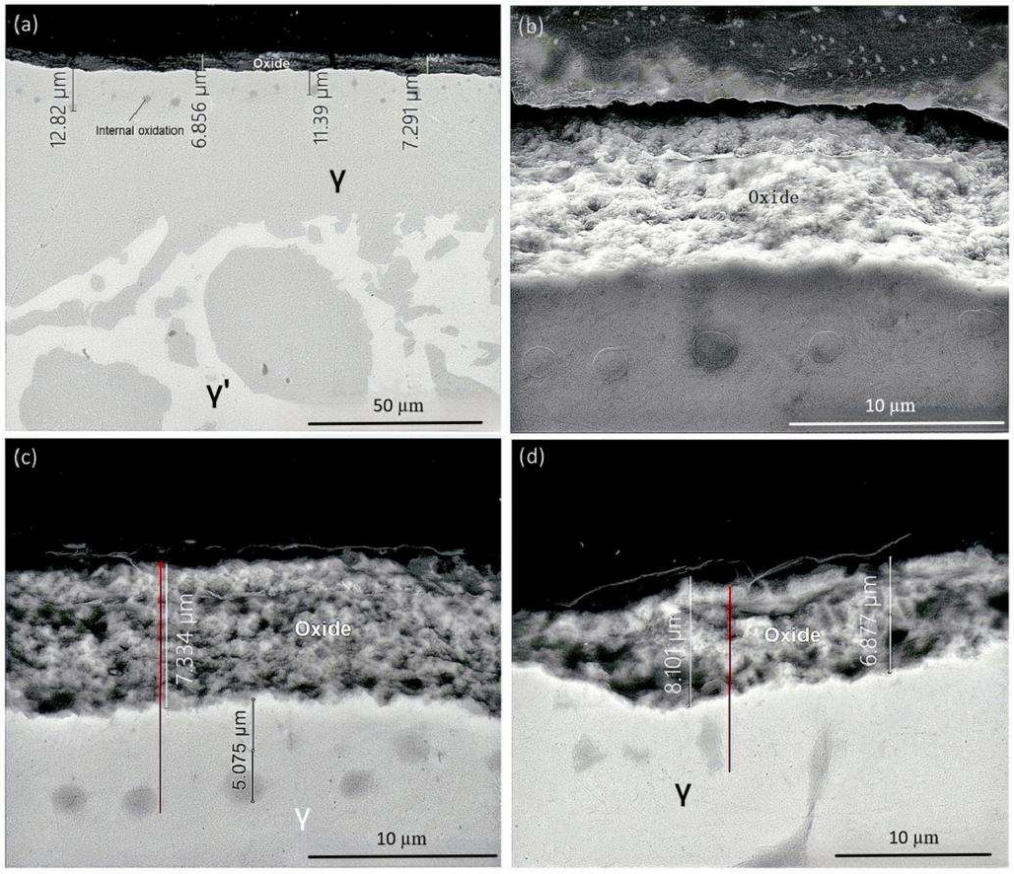

Figure 1. (Color online) (a) SEM/BSE images of cross sections of the Ni-20 at.% Al-5 at.% Pt specimen oxidized for 130 h under $PO_2 = 0.21$ bar at 1373 K presenting various districts; (b) SEM/SE (Second Electron) image of oxide morphology; (c) and (d) enlarged SEM/BSE images from (a); the red line in (c) and (d) shows the line scan for the EDS analysis.

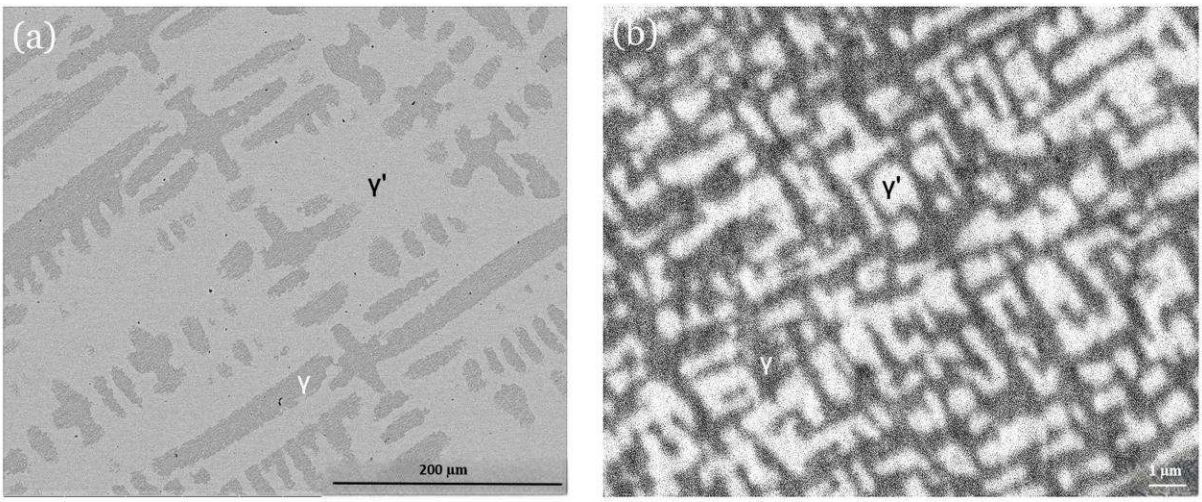

Figure 2. (Color online) SEM/BSE image of the microstructure in the Ni-20 at.% Al-5 at.% Pt alloy oxidized for 130 h under $PO_2 = 0.21$ bar at 1373 K. (a) SEM images of the γ'/γ morphology, (b) amplified morphology of the γ'/γ phase region.

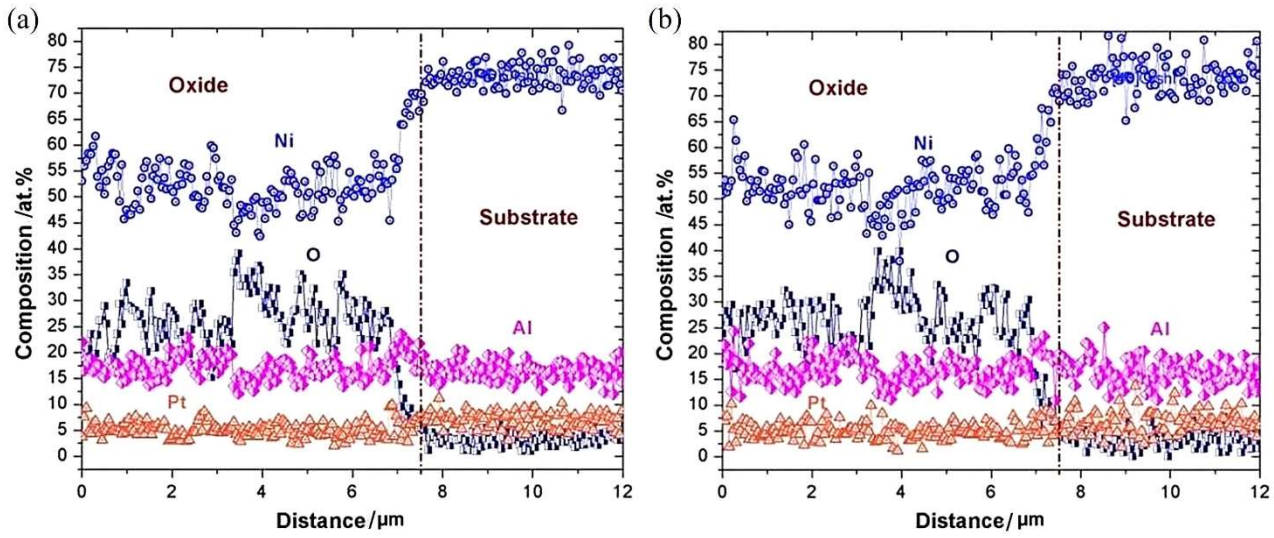

Figure 3. (Color online) EDS composition distribution curve of the SEM/BSE graphic. (a) Corresponds to Figure 1c, (b) corresponds to Figure 1d.

An additional EDS scan map of the SEM/BSE image in Figure 1d was conducted to show the comprehensive composition distribution of the different elements (Figure 4a). The distribution of Al, Ni, and O varies between the oxide layer and the matrix alloy, with localized concentration differences corresponding to distinct contrasts caused by different oxide phases. No significant differences were found in the distribution of Pt throughout the entire region. Based on the previous analysis, the grown oxide is actually a mixture of different oxidation compounds. One obvious region, marked with a red box in the EDS map, indicates the existence of an Al_2O_3 compound near the inner surface based on the element distribution.

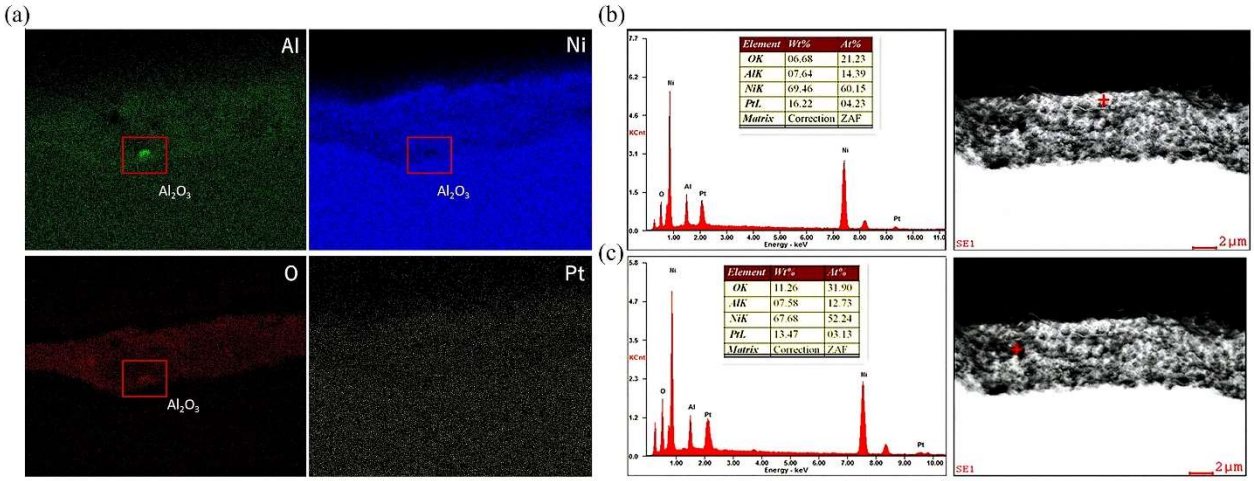

Figure 4. (Color online) (a) EDS composition distribution map of the SEM/BSE graphic corresponding to Figure 1d. (b) and (c) Composition point check (EDS analysis) of SEM/BSE graphics in Figure 1c.

EDS characterization of the grown oxide layer is shown in Figure 4b,c, where two points with different brightness contrasts were selected independently from the previous line scan in the SEM/BSE

image. This analysis indicates that there are at least two types of oxidation compounds within the TGO scale. Point detection demonstrates that both NiO and Ni-Al oxides formed on the samples, with the surface point in Figure 4a showing a higher concentration of nickel oxide, and the middle point in the oxide layer in Figure 4b showing a higher concentration of aluminum oxide.

The X-ray diffraction map of the grown oxide on the Ni-20 at.% Al-5 at.% Pt alloy after oxidation for 130 h at 1373 K is shown in Figure 5. The oxidation compounds in the TGO scale are primarily NiO mixed with γ-Ni and γ'-Ni_3Al. The diffraction peaks of γ' and γ phases are close to each other, with the exception of extra peaks from γ'. Peaks marked in blue indicate NiO, which may transform into spinel phases during further oxidation stages via a solid-phase reaction between Al_2O_3 and NiO in subsequent exposure. Al_2O_3 peaks were not detected, probably due to Al_2O_3 being present on the inner surface of the Ni-20 at.% Al-5 at.% Pt alloy in quantities too low to detect. The results from both EDS and XRD analysis show good consistency in illustrating the oxidation process.

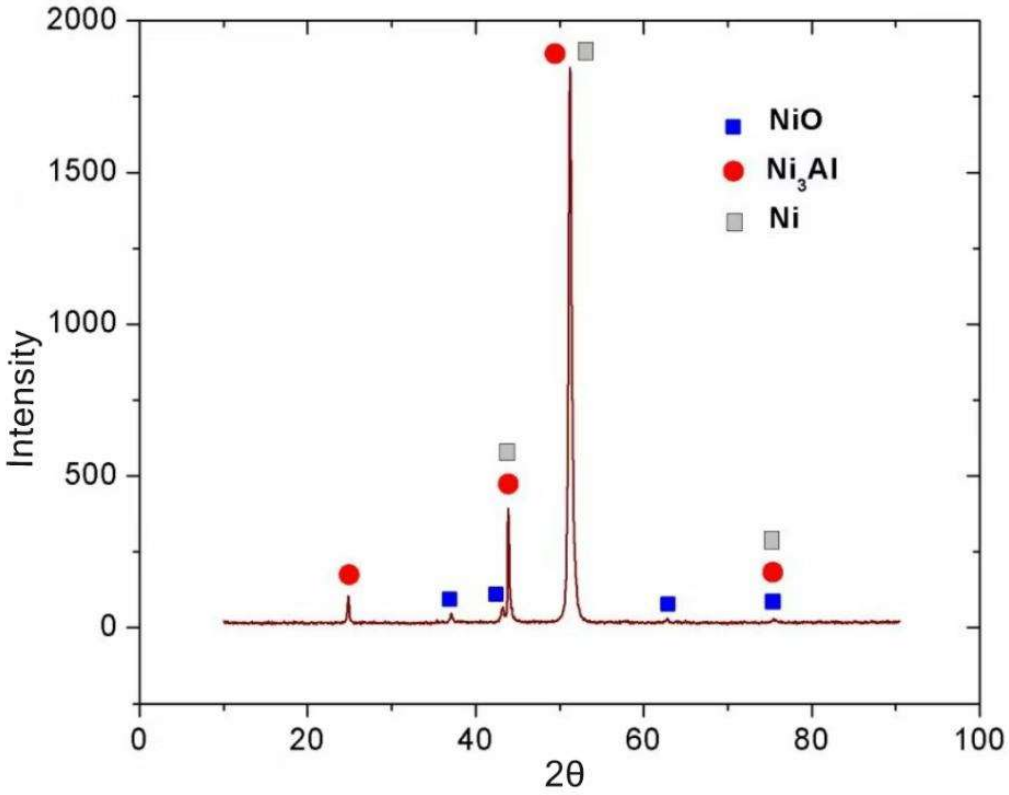

Figure 5. (Color online) XRD patterns of the grown oxide layer on the Ni-20 at.% Al-5 at.% Pt alloy oxidized for 130 h under a PO_2 = 0.21 bar at 1373 K.

3.2. Analysis based on thermodynamic calculations

As previously shown, a series of experimental characterizations were conducted to analyze the oxidation process of the Ni-20 at.% Al-5 at.% Pt alloy at 1373 K with PO_2 = 0.21 bar. In order to further comprehend the role of platinum in slowing down the oxidation process, thermodynamic calculations were performed for supplementary investigation. Figure 6 shows the calculated isothermal section at the current temperature in the nickel-rich region of the Ni-Al-Pt ternary alloy, based on the parameter assessments from [21]. The phase diagram presents the initial composition and relative

phase zone. Figure 7a presents the calculated phase fraction curves of γ and γ' in the Ni-Al-based alloy with varying Pt contents at 1373 K, using the thermodynamic database from [21] and Thermo-Calc software. The γ' content depends linearly on the Pt composition up to 20 at.% Pt, while the γ phase shows the opposite trend. Additionally, Figure 7b shows the variation curve for equilibrium concentrations of Al in γ' and γ phases vs. Pt content, revealing a slight decline in Al content with increasing Pt. Correspondingly, the equilibrium compositions of 5.477 at.% Pt in γ' phase and 4.103 at.% Pt in γ phase are achieved in the Ni-20 at.% Al alloy with 5 at.% Pt addition at the current temperature. This demonstrates that Al and Pt participate in the γ' phase.

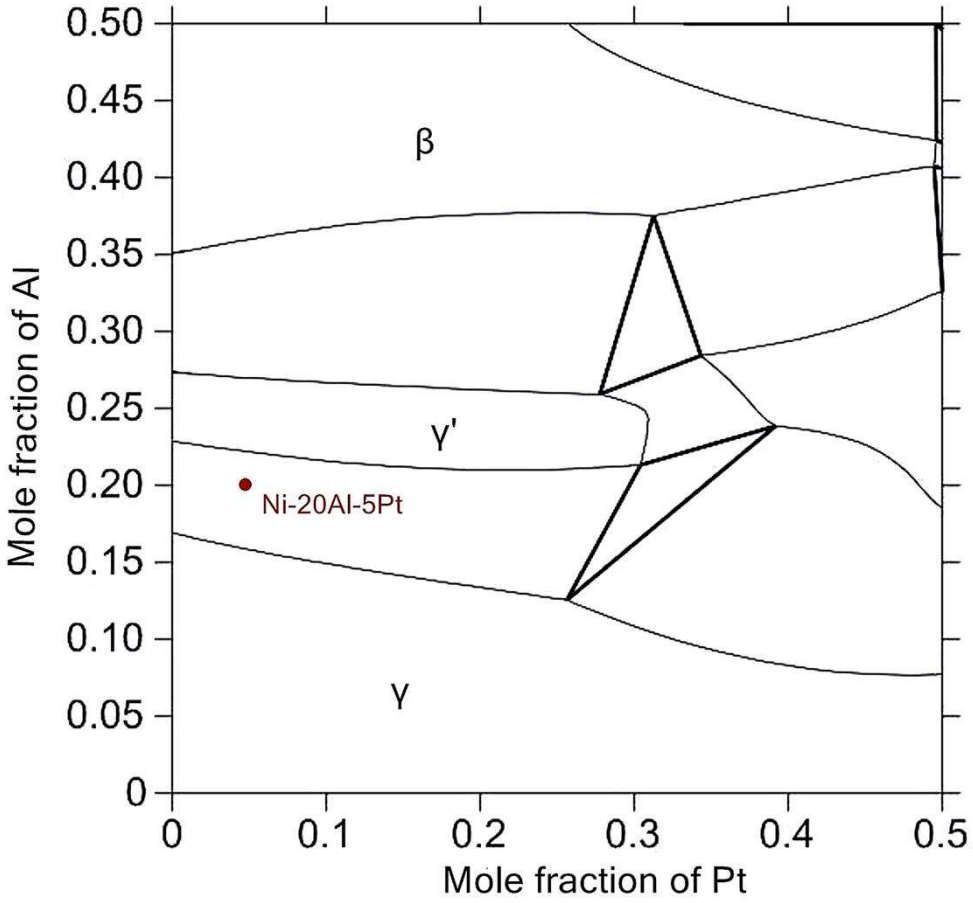

Figure 6. (Color online) Calculated isothermal section at 1373 K in the nickel-rich zone of Ni-Al-Pt ternary alloy based on the assessment descriptions from [21]. The original alloy constitute is appended in the figure.

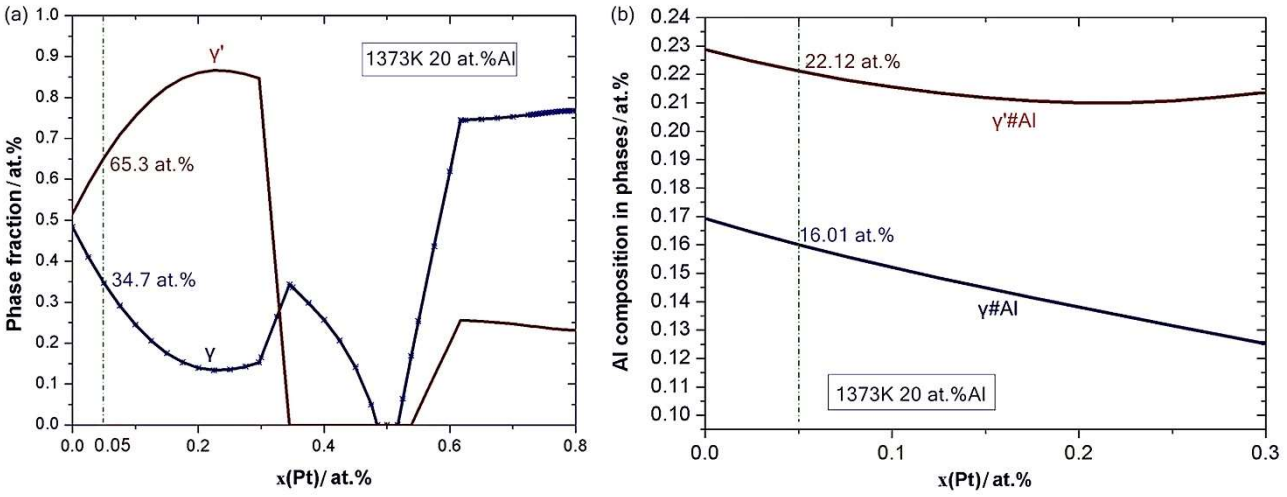

Figure 7. (Color online) Calculated (a) phase fractions of γ' and γ phases and (b) equilibrium aluminum compositions in γ' and γ vs. Pt contents in the Ni-20 at.% Al-based alloy with the addition of Pt (at.%) at 1373 K according to the database assessed by [21].

It is expected that uphill diffusion of aluminum from the matrix alloy in the TBC system occurs due to a reduction in Al chemical activity in phases with platinum content higher than 15 at.% [17]. To further explore this, the variation curve for the chemical activity of Al and Pt vs. Pt contents at 1373 K was calculated according to the thermodynamic database from [21], as shown in Figure 8. Both Al and Ni activities decrease with increased Pt content beyond 15 at.%, which explains the up-diffusion behavior. However, for the current Ni-20 at.% Al-based alloy with 5 at.% Pt, the chemical activity of nickel increased with the addition of Pt, as the Pt content is insufficient to inhibit the outward diffusion of Ni. This results in rapid NiO growth in the TGO scale, as observed in the previous experimental characterizations. When the Ni-Al-Pt alloy acts as the bond coat, increasing Pt content has two benefits. First, the enhanced up-diffusion effect ensures sufficient Al content in the Ni-Al-Pt bond coat, rather than interdiffusion depletion into the Ni-based substrate alloy. Second, at the initial oxidation stage of the bond coat, a diffusion concentration gradient of Al forms from the alloy to the oxidation interface; then, the presence of Pt and its up-diffusion effects on Al contribute to the enhanced transfer of Al to the oxidation interface. Both factors contribute to a stable and continuous development of the alumina oxide layer, with higher Pt contents yielding more stable alumina TGO.

The consumption of Al during Al_2O_3 formation is not compensated by outward Al diffusion from the alloy due to the low Pt content; this means that there is not an adequate driving force for the uphill diffusion of aluminum. The chemically favorable effect between Pt and Al is not noticeable at 5 at.% Pt. Increasing Pt content above 15 at.% contributes to the establishment of Al_2O_3 scales by inhibiting the formation of rapid NiO growth, as shown in Figure 8. This increase in Al at the oxide/substrate interface results in the development of a more robust Al_2O_3 layer on the alloy surface.

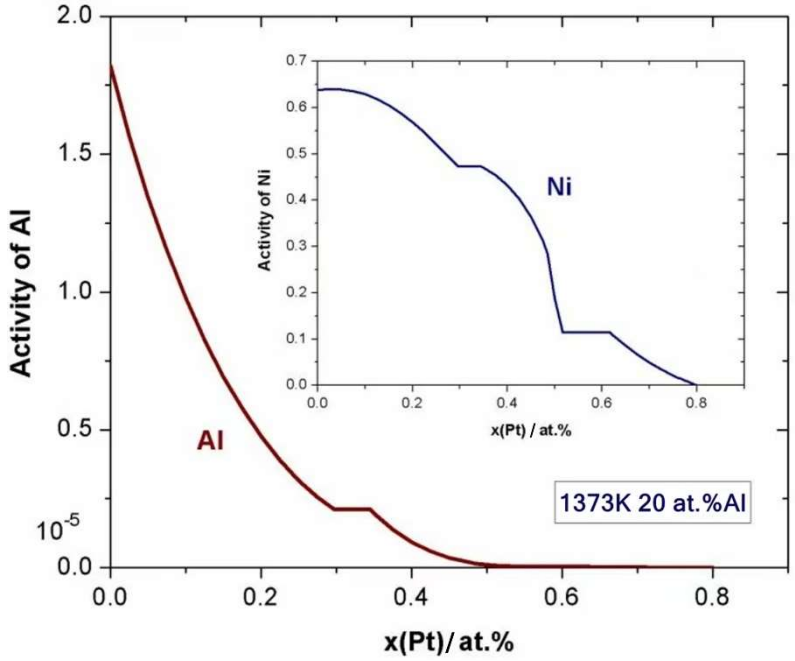

Figure 8. (Color online) Chemical activity of aluminum and nickel vs. Pt contents in Ni-20 at.% Al-5 at.% Pt at 1373 K obtained according to the thermodynamic database from [21].

The oxidation process follows the formation energy of oxides, as presented in Figure 9, which shows the standard formation energy vs. temperature for Al_2O_3 and NiO. At the experimental temperature of 1373 K, NiO is less stable than Al_2O_3 in the standard state, so Al will preferentially be oxidized beneath the NiO layer as long as its composition and chemical activity are above critical values.

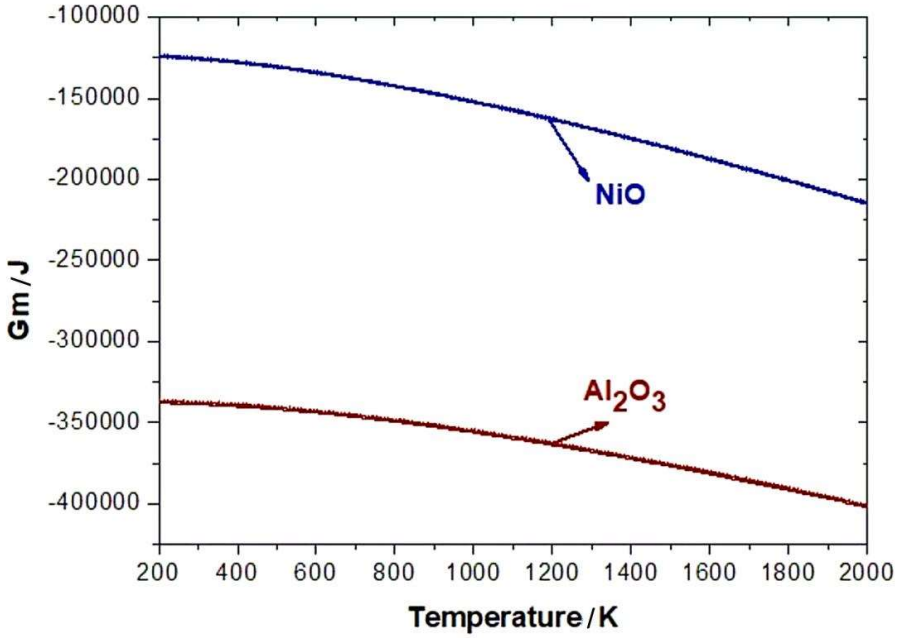

Figure 9. (Color online) Schematic diagram of the standard formation energy vs. temperature for Al_2O_3 and NiO calculated based on our previous work [22,23].

A schematic of the oxidation process of the Ni-20 at.% Al-based alloy with 5 at.% Pt is shown in Figure 10. Generally, oxidation can be divided into two types: anion diffusion and cation diffusion [24]. The former involves oxygen anion conveyance, and the latter involves metal ion conveyance. Metal ions usually oxidize from the free surface, while oxygen ions develop oxides from the alloy surface. The whole oxidation process can be summarized in four steps:

(1) As shown in Figure 10a,b, in the initial stage, Al_2O_3 develops initially on the underside, while NiO grows on top and disrupts the alumina. This occurs due to NiO expanding faster than Al_2O_3, as shown in prior investigations on the oxidation kinetics of pure Al [22] and pure Ni [23]. The ion mobility of NiO is faster than that of Al_2O_3. During the initial period, NiO expands fast and dominates the oxidation kinetics, allowing Al_2O_3 grains to be embedded into the NiO scale. As Ni oxide expands, meta-stable θ-Al_2O_3 with loose porous morphology quickly develops its own scales below the Ni oxide layer. In Al_2O_3, O ions diffusion predominates, and NiO primarily diffuses Ni ions.

(2) The development of NiO contributes to Ni depletion and Al accumulation. When Al reaches a threshold, θ-Al_2O_3 converts to α-Al_2O_3 with a compressed configuration. Outward diffusion of Al predominates, with inward diffusion of O playing a secondary role, according to prior research [22,23]. This α-Al_2O_3 layer may form an entire scale to prevent further Ni outward diffusion.

(3) If Al content becomes insufficient, NiO can react with Al_2O_3 to generate damaging $NiAl_2O_4$.

(4) The continued oxidation process can lead to Ni aggregation at the oxide layer/substrate alloy interface. The opposite-directional diffusion of Ni is larger than the transportation of Al to the interface [25,26]. Namely, vacancies accumulate by unbalanced diffusion of Al toward the Al_2O_3 layer and opposite-directional diffusion of Ni according to the flux balance reaction, $J_V = J_{Ni} - J_{Al}$. These vacancies may coalesce into small voids, causing widespread oxide layer spallation. As shown here, Pt improves Al diffusion and reduces the opposite-directional diffusion flux of nickel, thereby decreasing the diffusion flux of outward vacancies and resulting in a thinner, more rupture-resistant oxide layer.

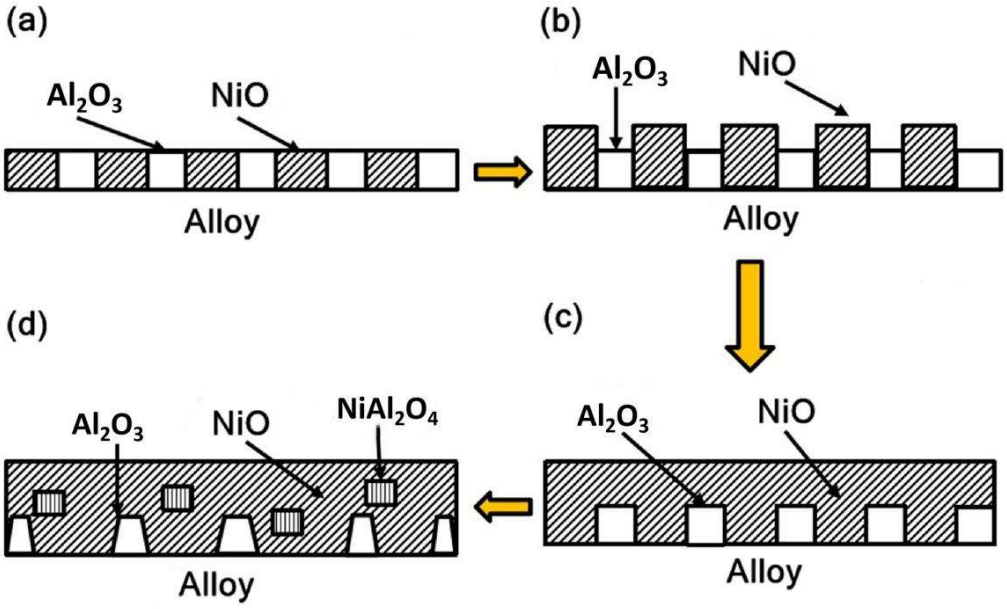

Figure 10. (Color online) Sketch map of the oxidized procedure of the Ni-20 at.% Al-based alloy with 5 at.% Pt addition.

4. Conclusions

Oxidation experiments were conducted in a Ni-20 at.% Al-based alloy with 5 at.% Pt addition at 1373 K. Relative thermodynamic calculations were performed to further comprehend the oxidation mechanism of Ni-Al alloys with different Pt contents. From there, the effects of alloy constitutes on the oxidative development of the TGO layers were discussed. The primary conclusions are as follows:

(1) Initially, Al_2O_3 granules form within the NiO scale. Here, O ion diffusion drives the development of Al_2O_3, while Ni cation diffusion drives NiO growth.

(2) The development of NiO leads to Ni depletion and Al accumulation, leading to the transformation of θ-Al_2O_3 into α-Al_2O_3 with a compacted configuration. The outward Al diffusion then predominates, followed by the inward diffusion of oxygen. The α-Al_2O_3 layer may restrict further outward permeation of Ni.

(3) The formation of $NiAl_2O_4$, combined with vacancy accumulation and coalescence into voids, results in widespread oxide layer rupture due to unbalanced diffusion of Ni and Al. Platinum mitigates this rupture process by reducing the net diffusion flux of vacancies, leading to a thinner and more stable oxide layer.

Use of AI tools declaration

The authors declare they have not used Artificial Intelligence (AI) tools in the creation of this article.

Acknowledgments

The authors acknowledge the financial support received from the National Natural Science Foundation of China (Grant No. 52101004) and the Fundamental Research Funds for the Central Universities (Grant No. FRF-TP-20-047A1), the financial support from China Postdoctoral Science Foundation (Grant No.2020M680341) is also acknowledged.

Author contributions

Na Ta is involved in conceptualization, methodology and calculations, writing original draft, resources, funding acquisition. Lijun Zhang is involved in review and editing and discussion. Qin Li is involved in methodology and validation.

Conflict of interest

The authors declare no conflict of interest.

References

1. Padture NP, Gell M, Jordan EH (2002) Thermal barrier coatings for gas-turbine engine applications. *Science* 12: 280–284. https://doi.org/10.1126/science.1068609
2. Smialek JL, Lowell CE (1974) Effects of diffusion on aluminum depletion and degradation of NiAl Coatings. *J Electrochem Soc* 121: 800–805. https://doi.org/10.1149/1.2401922

3. Zhao X, Liu J, Rickerby DS, et al. (2011) Evolution of the interfacial toughness of thermal barrier system with a Pt-diffused γ+γ' bond coat. *Acta Mater* 59: 6401–6411. https://doi.org/10.1016/j.actamat.2011.07.001
4. Zhou B, He J, Liu L, et al. (2022) The interaction between Dy, Pt and Mo during the short-time oxidation of (γ'+β) two-phase NiAl coating on single crystal superalloy with high Mo content. *Surf Coat Tech* 430: 127999. https://doi.org/10.1016/j.surfcoat.2021.127999
5. Liu C, Chen Y, Qiu L, et al. (2020) The al-enriched γ'-Ni_3Al-base bond coat for thermal barrier coating applications. *Corros Sci* 167: 108523. https://doi.org/10.1016/j.corsci.2020.108523
6. Hayashi S, Wang W, Sordelet DJ (2005) Interdiffusion behavior of Pt-modified γ-Ni + γ′-Ni_3Al alloys coupled to Ni-Al-based alloys. *Metall Mater Trans* 36: 1769–1775. https://doi.org/10.1007/s11661-005-0041-3
7. Terock M, Fleischmann E, Hochmuth C (2013) Synthesis and characterization of a Pt-Al-Cr-Ni γ/γ′-coating on the Ni-based superalloy CMSX-4. *Surf Coat Tech* 236: 347–352. https://doi.org/10.1016/j.surfcoat.2013.10.011
8. Gleeson B, Wang W, Hayashi S (2004) Effects of platinum on the interdiffusion and oxidation behavior of Ni-Al-Based alloys. *Mater Sci Forum* 461–464: 213–222. https://doi.org/10.4028/www.scientific.net/MSF.461-464.213
9. Ali AI, Dad CA (2023) Analysis and evolution on diffusional stability of nickel aluminide bond coat via nickel electro-plating. *Eur Phys J Plus* 138: 229. https://doi.org/10.1140/epjp/s13360-023-03816-6
10. Oskay C, Galetz MC, Murakami H (2019) Mechanical behaviour of conventional, Pt- and Pt/Ir-modified nial diffusion coatings after thermocyclic exposure at 1100 °C. *Mat High Temp* 36: 404–416. https://doi.org/10.1080/09603409.2019.1591064
11. Bai M, Chen Y, Sun Y, et al. (2021) Mitigation of platinum depletion in platinum diffused single phase bond coat on CMSX-4 superalloy. *Coatings* 11: 669–682. https://doi.org/10.3390/coatings11060669
12. Svensson H, Christensen M, Knutsson P (2009) Influence of Pt on the metal–oxide interface during high temperature oxidation of NiAl bulk materials. *Corros Sci* 51: 539–546. https://doi.org/10.1016/j.corsci.2008.12.016
13. Shirvani K, Firouzi S, Rashidghamat A (2012) Microstructures and cyclic oxidation behaviour of Pt-free and low-Pt NiAl coatings on the Ni-base superalloy Rene-80. *Corros Sci* 55: 378–384. https://doi.org/10.1016/j.corsci.2011.10.037
14. Yamashita T, Sato N, Fukumoto M (2015) Preparation of Ni-Al-Pt coating on Ni-6 at%Cr alloy by electrodeposition method and cyclic-oxidation resistance. *Mater Trans* 56: 1207–1213. https://doi.org/10.2320/MATERTRANS.M2015051
15. Hou PY, Tolpygo VK (2007) Examination of the platinum effect on the oxidation behavior of nickel-aluminide coatings. *Surf Coat Tech* 202: 623–627. https://doi.org/10.1016/j.surfcoat.2007.06.013
16. Luis CD, Alvaradoorozco J, Ruizluna H (2016) Study of the isothermal oxidation process and phase transformations in B2-(Ni,Pt)Al/RENE-N5 system. *Metals* 6: 208. https://doi.org/10.3390/met6090208
17. Izumi T, Gleeson B (2007) Oxidation resistance of Pt containing γ-Ni+γ′-Ni_3Al alloys. *J Jpn I Met* 71: 34–40. https://doi.org/10.2320/jinstmet.71.34

18. Pint BA, Haynes JA, More KL, et al. (2008) The performance of Pt-modified alumina-forming coatings and model alloys. *Superalloys* 641–650.
19. Chen Y, Zhao X, Bai M, et al. (2015) Effect of platinum addition on oxidation behaviour of γ/γ′ nickel aluminide. *Acta Mater* 86: 319–330. https://doi.org/10.1016/j.actamat.2014.12.023
20. Nan M (2007) High temperature oxidation behavior of γ-Ni+γ'-Ni_3Al alloys and coatings modified with Pt and reactive elements. *PhD Dissertation*, Iowa State University. https://doi.org/10.2172/933131
21. Liu XL, Lindwall G, Otis R, et al. (2016) Thermodynamic remodeling of the Al-Pt system towards an assessment of the Al-Ni-Pt system. *Calphad* 55: 88–102. https://doi.org/10.1016/j.calphad.2016.08.002
22. Ta N, Zhang LJ, Li Q, et al. (2018) High-temperature oxidation of pure Al: Kinetic modeling supported by experimental characterization. *Corros Sci* 135: 355–369. https://doi.org/10.1016/j.corsci.2018.05.013
23. Xing F, Ta N, Zhong J, et al. (2019) Kinetic modeling of high-temperature oxidation of pure nickel. *Solid State Ionics* 341: 115018. https://doi.org/10.1016/j.ssi.2019.115018
24. Shreir LL, Jarman RA, Burstein GT (1963) *Corrosion*. Butterworth-Heinemann Ltd, Oxford.
25. Janssen MMP, Rieck GD (1968) Reaction diffusion and Kirkendall-effect in the nickel-aluminum system. *Trans Metall Soc AIME* 239: 1372–1385.
26. Angenete J, Stiller K (2003) Oxidation of simple and Pt-modified aluminide diffusion coatings on Ni-base superalloys-II. oxide scale failure. *Oxid Met* 60: 83–101. https://doi.org/10.1023/A:1024617313726

AIMS Press